# Temperature dependent pulsed IV and RF characterization of B-(Al<sub>x</sub>Ga<sub>1-x</sub>)<sub>2</sub>O<sub>3</sub>/Ga<sub>2</sub>O<sub>3</sub> hetero-structure FET with **ex situ** passivation

Cite as: Appl. Phys. Lett. **120**, 172102 (2022); https://doi.org/10.1063/5.0083657 Submitted: 28 December 2021 • Accepted: 10 April 2022 • Published Online: 25 April 2022

🗓 Chinmoy Nath Saha, 🗓 Abhishek Vaidya and 🗓 Uttam Singisetti

#### **COLLECTIONS**

Paper published as part of the special topic on Wide- and Ultrawide-Bandgap Electronic Semiconductor Devices







ARTICLES YOU MAY BE INTERESTED IN

SnO/ $\beta$ -Ga<sub>2</sub>O<sub>3</sub> heterojunction field-effect transistors and vertical p–n diodes Applied Physics Letters **120**, 112110 (2022); https://doi.org/10.1063/5.0083032

Schottky diode characteristics on high-growth rate LPCVD  $\beta$ -Ga<sub>2</sub>O<sub>3</sub> films on (010) and (001) Ga<sub>2</sub>O<sub>3</sub> substrates

Applied Physics Letters 120, 122106 (2022); https://doi.org/10.1063/5.0083659

 $\beta$ -Gallium oxide power electronics

APL Materials 10, 029201 (2022); https://doi.org/10.1063/5.0060327

## Lock-in Amplifiers up to 600 MHz









### Temperature dependent pulsed IV and RF characterization of b-(Al<sub>x</sub>Ga<sub>1-x</sub>)<sub>2</sub>O<sub>3</sub>/Ga<sub>2</sub>O<sub>3</sub> hetero-structure FET with ex situ passivation

Cite as: Appl. Phys. Lett. 120, 172102 (2022); doi: 10.1063/5.0083657

Submitted: 28 December 2021 · Accepted: 10 April 2022 ·

Published Online: 25 April 2022









Chinmoy Nath Saha, (1) (a) Abhishek Vaidya, (b) and Uttam Singisetti (b)



#### **AFFILIATIONS**

Department of Electrical Engineering, University at Buffalo, Buffalo, New York 14240, USA

Note: This paper is part of the APL Special Collection on Wide- and Ultrawide-Bandgap Electronic Semiconductor Devices. <sup>a)</sup>Author to whom correspondence should be addressed: chinmoyn@buffalo.edu

#### **ABSTRACT**

In this work, we report a study of the temperature dependent pulsed current voltage and RF characterization of b-(Al<sub>x</sub>Ga<sub>1-x</sub>)<sub>2</sub>O<sub>3</sub>/Ga<sub>2</sub>O<sub>3</sub> hetero-structure FETs (HFETs) before and after silicon nitride (Si<sub>3</sub>N<sub>4</sub>) passivation. Under sub-microsecond pulsing, a moderate DC-RF dispersion (current collapse) is observed before passivation in gate lag measurements, while no current collapse is observed in the drain lag measurements. surements. The dispersion in the gate lag is possibly attributed to interface traps in the gate-drain access region. DC-RF dispersion did not show any strong dependence on the pulse widths. Temperature dependent RF measurements up to 250 °C do not show degradation in the cutoff frequencies. After Si<sub>3</sub>N<sub>4</sub> deposition at 350 °C, a shift of the threshold voltage is observed which changed the DC characteristics. However, the current collapse is eliminated; at 200 ns pulse widths, a 50% higher current is observed compared to the DC at high drain voltages. No current collapse is observed even at higher temperatures. RF performance of the passivated devices does not show degradation. These results show that ex situ deposited Si<sub>3</sub>N<sub>4</sub> is a potential candidate for passivation of b-(Al<sub>x</sub>Ga<sub>1-x</sub>)<sub>2</sub>O<sub>3</sub>/Ga<sub>2</sub>O<sub>3</sub> HFETs.

Published under an exclusive license by AIP Publishing. https://doi.org/10.1063/5.0083657

b-Ga<sub>2</sub>O<sub>3</sub> is an extensively investigated ultra-widebandgap semiconductor for next generation power electronics and RF applications because of its favorable material properties. Due to its larger calculated Baliga figure of merit (BFoM), it has been explored for high voltage power devices. Several groups have reported transistors and diodes with kV range breakdown voltages<sup>3-7</sup> further validating its potential. Additionally, due to its high calculated electron saturation velocities,8 b-Ga<sub>2</sub>O<sub>3</sub> (Ga<sub>2</sub>O<sub>3</sub>) has a higher Johnson's figure of Merit (JFoM) making it attractive for potential RF applications such as high power amplifiers and GHz switches. Due to its large bandgap, Ga2O3 devices can also operate at higher temperatures. Both MOSFETs and MESFET devices with high frequency have been reported.<sup>9,10</sup> Recently, a record current gain cut off frequency (f<sub>T</sub>) of 30 GHz and a power gain cut off frequency (f<sub>MAX</sub>) of 37 GHz have been reported for b-(Al<sub>0.19</sub>Ga<sub>0.81</sub>)<sub>2</sub>O<sub>3</sub>/Ga<sub>2</sub>O<sub>3</sub> (AlGaO/GaO) hetero-structure FETs (HFETs)<sup>11</sup> with ultra-scaled gate lengths and regrown Ohmic contacts.

Another important aspect of high frequency performance of a device is DC-RF dispersion. This is typically characterized by a decrease in the drain current and trans-conductance in unpassivated devices at higher frequencies resulting in lower RF output power. The

DC-RF dispersion or current collapse is caused by the finite amount of time taken by any traps, located either at an air/device interface in a gate drain access region or in the bulk semiconductor under the gate in response to either gate or drain voltage transients. Pulsed current voltage (IV) measurements are popular method to analyze the DC-RF dispersion and to identify the location of the traps. 12-15

There have been a number of studies on the pulsed IV characterization for Ga<sub>2</sub>O<sub>3</sub> devices. Wong et al. <sup>16</sup> reported no current collapse at 100 ls pulse width with SiO2 passivation in high voltage devices. Moser et al.<sup>17</sup> reported large signal power performance with continuous and pulsed conditions<sup>17,18</sup> and found that the interface trap in the gate drain region is the source of dispersion. Singh et al. 19 reported that Al<sub>2</sub>O<sub>3</sub>/SiO<sub>2</sub> passivated devices do not show any current collapse at 1 ls pulse width at room temperature. McGlone et al. 20-22 explored buffer traps in delta doped MESFETs using the double pulsed IV condition. Joishi et al.<sup>23</sup> used 5 ls double pulsed measurement to show that *in situ* passivation by an UID Ga<sub>2</sub>O<sub>3</sub> layer can improve the current significantly even though the channel was exposed to reactive ion etching (RIE). However, submicrosecond pulsed IV is necessary to understand the device performance at GHz frequencies as is the case for AlGaN/GaN devices.

Recently, sub-microsecond pulsed-IV characterization of gate recessed Ga<sub>2</sub>O<sub>3</sub> MOSFETs was reported, which shows severe DC-RF dispersion in unpassivated devices. <sup>25</sup> Although dispersion was reduced (50%) after silicon nitride (Si<sub>3</sub>N<sub>4</sub>) passivation, it was not eliminated. It is important to completely eliminate current collapse in Ga<sub>2</sub>O<sub>3</sub> devices to achieve the predicted RF performance. In this work, we report a temperature dependent pulsed IV characterization of AlGaO/GaO HFETs. We show that *ex situ* deposited Si<sub>3</sub>N<sub>4</sub> passivation can eliminate current collapse up to 200 ns pulse widths. We also report the temperature dependent high frequency performance of AlGaO/GaO HFETs.

A cross section schematic of the completed AlGaO/GaO HFET is shown in Fig. 1(a). Details of ozone MBE growth and device fabrication are discussed in Refs. 11 and 26. The salient features of the device are the use of source/drain regrowth for contacts and the absence of any RIE exposure to the device access regions. It has been reported that RIE damage to the channel layer can cause surface traps resulting in significant DC-RF dispersion. 18,25 The gate length (L<sub>G</sub>) was scaled to 160-200 nm, and the source access distance (LsG) was scaled down to 55 nm using electron beam lithography. After pre-passivation electrical characterization, a 300 nm thick low stress Si<sub>3</sub>N<sub>4</sub> was deposited using plasma enhanced chemical vapor deposition (PECVD) at 350 °C temperature with 20 sccm SiH<sub>4</sub> and 30 sccm NH<sub>3</sub> at 1900 mTorr pressure. Standard solvent clean was carried out before the deposition. Finally, Si<sub>3</sub>N<sub>4</sub> was removed using CF<sub>4</sub> based RIE on top of the contacts for electrical characterization. The contacts have a co-planar waveguide (CPW) layout for high frequency measurements.

Figure 1(b) shows the output characteristics of a 160 nm gate length unpassivated device at room temperature and 250 °C, and the device shows a normally off behavior (V<sub>th</sub> 1/4 0.5 V) with lower drain current at higher temperatures. The reduction in the drain current at higher temperatures is due to the reduction in the channel mobility at higher temperatures. For DC-RF dispersion studies, gate lag, drain lag, and double pulsed measurements were carried out. In the drain lag, the drain was pulsed from the off state (0 V) to the on state (5 or 7 V) (referred to as drain turn-on) while the gate bias was constant. For gate lag, the gate terminal was pulsed from the off state (below V<sub>th</sub>) to the on state (referred to as gate turn-on) while maintaining a constant drain bias. Finally, for a double pulsed technique, both gate and drain were pulsed from the off state to the on state (or vice versa) and a combination of on and off biases. The pulsed IV measurement was carried

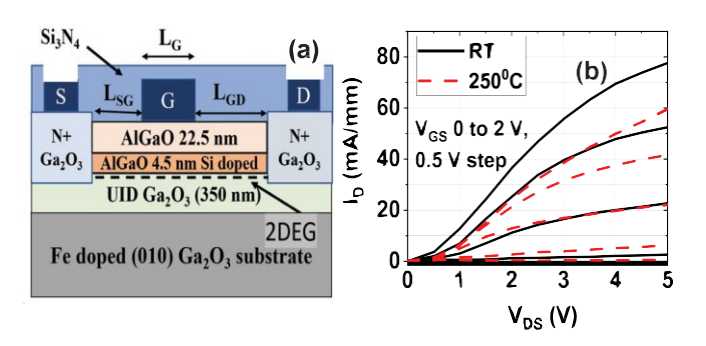


FIG. 1. (a) Final cross section of a device after passivation. The gate metal stack is Pt/Au  $^{1}$ /4 20/180 nm and (b) DC output curve for a device (L<sub>G</sub>  $^{1}$ /4 160 nm) at room temperature and 250 °C.

out using an Auriga AU-5 high voltage Pulsed IV setup with 20 nanosecond (ns) rise and fall time, and the pulse width was varied from 1 ms to  $200\,\mathrm{ns}$  with low duty cycle (<1%). The system was calibrated at each temperature before measuring the devices. The drain current collapse is quantified by

$$DI_{cc} \frac{I_{d;DC} - I_{d;PW}}{I_{d;DC}}; \qquad (1)$$

where  $I_{d,DC}$  is the drain current value during DC measurement and  $I_{d,PW}$  is the drain current measured at the corresponding pulse width. The gate current was monitored during the pulsed measurements and was always very low compared to the drain current.

Drain lag measurements are used to study buffer traps/bulk traps in the device as they respond to a drain pulse.<sup>27</sup> Figure 2(a) shows the DC and drain turn-on measurements of the unpassivated device at constant gate bias, and negligible dispersion is observed. A slight increase in the current is observed at smaller pulse widths, which could be due to the reduced self-heating effect. These measurements rule out the presence of any buffer traps as was the case for ozone MBE grown MOSFET devices.<sup>25</sup> Figure 2(b) shows the DC and gate pulsed output curve of the same device; as seen in the figure, a moderate DC-RF dispersion or current collapse (22%) is observed. The recessed channel MOSFETs by Vaidya and Singisetti had increasing DC-RF dispersion with decreasing pulse width, and 60% current collapse was reported at 200 ns pulse width. Yet here, we observe that the amount of current collapse does not depend strongly on the pulse widths. The dispersion can be attributed to the interface traps either under the gate or in the gate drain access region forming a virtual gate. 13-15 Figure 2(c) shows

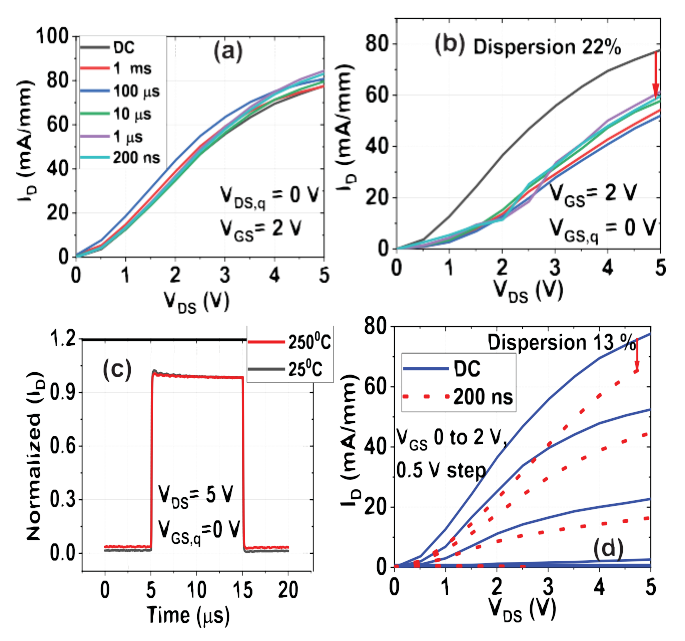


FIG. 2. (a) Drain lag/pulse measurement at V<sub>GS</sub>  $\frac{1}{4}$  2 V showing no DC-RF dispersion, (b) gate lag measurement at V<sub>GS</sub>  $\frac{1}{4}$  2 V showing DC-RF dispersion, (c) temperature dependent I<sub>D</sub> pulse shape for 10 Is gate turn on pulse measured at V<sub>GS</sub>  $\frac{1}{4}$  2 V before passivation, and (d) double pulse measurement (V<sub>GS,q</sub>  $\frac{1}{4}$  0 V, V<sub>DS,q</sub>  $\frac{1}{4}$  0 V) showing reduced current collapse at room temperature.

the measured drain current transient for the 10 ls pulse gate turn-on signal, and the pulse shows fast drain current turn-on and turn-off. This is in contrast to the recessed channel MOSFETs, <sup>25</sup> where slow turn-on and turn-off was observed which was attributed to RIE induced traps. The observed pulse shape explains why the DC-RF dispersion does not depend on pulse widths. The pulse shape remains unchanged even at 250°C as seen in Fig. 2(c).

Double pulsed IV-measurements, where both the drain and gate are pulsed from different gate and drain quiescent points (V<sub>GS,q</sub>, V<sub>DS,q</sub>), can simulate the device conditions during its operation as an amplifier or switch, thus provide more insight. Figure 2(d) compares the DC and double pulsed output characteristics, and  $V_{GS,q}$  1/4 0 and  $V_{DS,q}$  1/4 0 were used to minimize self-heating effects. At the highest pulsed or nonquiescent gate bias (V<sub>GS,ng</sub> ½ 2 V), a low dispersion of 13% is observed, which is lower than the current collapse in the gate pulsed measurements. This current collapse is attributed to the possible traps in the gate-drain access region that were responsible to the current collapse seen in Fig. 2(b). Here, the dispersion was observed without a finite gate-drain bias in the quiescent condition. The traps could be charged due to the built-in bias or charged after pulses have been applied. Further analysis is needed in the future to fully understand the origin of this. Double pulsed I<sub>DS</sub>-V<sub>GS</sub> transfer curves (see the supplementary material) using different quiescent bias conditions did not show any change in the threshold voltage ruling out traps under the gate, 14,19,28 leaving the gate-drain access region interface traps as the likely source of the observed dispersion. It is noted that the presence of deep-level traps is not probed in these pulsed IV measurements.

Figure 3(a) shows the measured current collapse as a function pulse width for different quiescent gate and drain biases. All  $I_D$  values were measured at  $V_{GS}$  ½ 2V and  $V_{DS}$  ½ 5V for this calculation. The

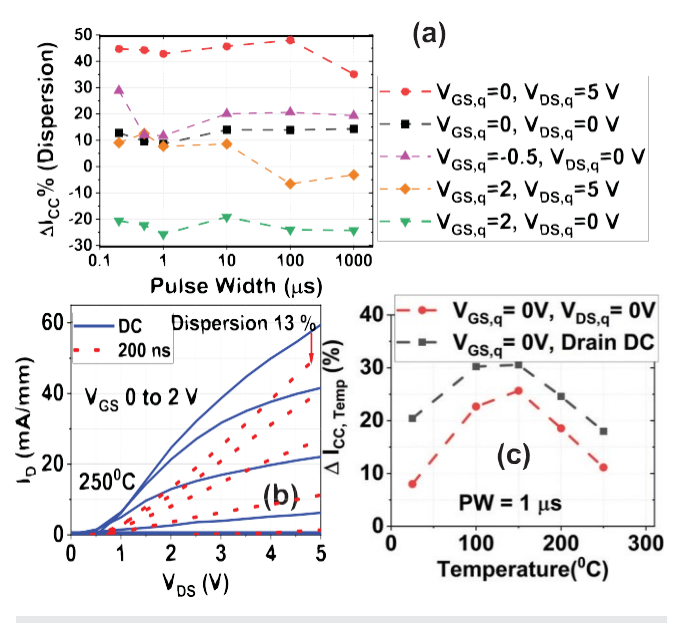


FIG. 3. (a) Comparison of current collapse for output curves at different quiescent bias conditions before passivation (L $_{\rm G}$   $^{1}$ 4 160 nm), (b) DC and pulsed IV curve (V $_{\rm GS,q}$   $^{1}$ 4 0 V, V $_{\rm DS,q}$   $^{1}$ 4 0 V) at 250 °C showing similar dispersion at room temperature, and (c) temperature dependent dispersion for 1 Is PW showing lower current collapse for the double pulsed technique.

maximum current collapse (40%) is observed for  $V_{GS,q}$  ¼ 0V and  $V_{DS,q}$  ¼ 5V; the larger gate–drain voltage and pinch off condition lead to longer virtual gate formation, hence the increased current collapse. In contrast, for  $V_{GS,q}$  ¼ 2V and  $V_{DS,q}$  ¼ 0V, no current collapse is observed, instead a small increase in the current is seen. In this condition, the device is in the on state, and the traps are filled, which eliminated the current collapse, <sup>17</sup> while the reduced self-heating in pulsed conditions likely leads to a slight increase in the current.  $V_{GS,q}$  ¼ -0.5 V gave a higher dispersion compared to the  $V_{GS,q}$  ¼ 0 quiescent condition, because more negative voltage causes more trapping and higher current collapse. The response of other quiescent conditions is an interplay of trapping and self-heating effects.<sup>29</sup>

Temperature dependent pulsed IV measurements were also carried out up to 250 °C. As seen in Fig. 3(b), a low current collapse of 13% is observed at 250 °C for 200 ns pulse width similar to the case at room temperature. Drain lag, gate lag, and double pulsed measurements at higher temperatures show a similar trend as room temperature for the DC-RF dispersion (similar to Fig. 2). Figure 3(c) shows the double pulsed current collapse at 1 ls pulse width as a function of temperature. It shows a non-monotonic behavior with temperature with highest dispersion at 150 °C. This trend is the result of complex interplay of several effects including trapping self-heating effects and the stage temperature. With an increase in temperature, traps can respond faster, while the self-heating effects could be reduced because of overall decrease in the current at higher temperatures [see Fig. 1(b)]. A more careful analysis, including thermal simulations, is needed to fully understand the temperature dependent pulsed IV data.

In order to eliminate the observed current collapse in the AlGaO/GaO HFETs, a Si<sub>3</sub>N<sub>4</sub> passivation was investigated. It has been used to reduce or eliminate DC-RF dispersion/current collapse in AlGaN/GaN devices. <sup>30-33</sup> Interestingly, after passivation, a significant change in the threshold voltage to -1 V is observed (see the supplementary material). It is attributed to possible intermixing of Au and Pt in the gate stack, resulting in a lower Schottky barrier, although introduction of traps under gate is not completely ruled out. Intermixing of Pt and Au at 200 °C is reported in Ref. 34. The DC output characteristics of a HFET after passivation are shown in Fig. 4(a). The decreased DC drain current and transconductance can be attributed to increased sheet

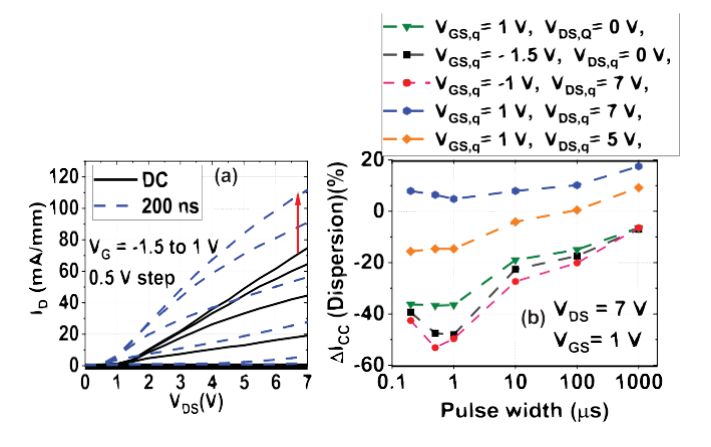


FIG. 4. (a) Output curve ( $L_{\rm G}$  ½ 200 nm) after passivation ( $V_{\rm GS,q}$  ½ -1.5 V,  $V_{\rm DS,q}$  ½ 0 V) using the double pulse method and (b) comparison of current collapse at the double pulse method using different quiescent bias conditions after passivation.

resistance in the access regions due to plasma damage during  $Si_3N_4$  deposition at  $350\,^{\circ}\,\mathrm{C}$ , which is higher than previous reports.  $^{25,35}$  In addition, as seen in the DC curves, the contact linearity has changed. All these changes in the DC characteristics need to be eliminated in an ideal passivation scheme. Further optimization of the  $Si_3N_4$  process is required. In the subsequent analysis, the pulsed measurements are from  $V_{GS}$ –1.5 to 1 V (pinch off to the on state) to keep comparable gate overdrive ( $V_{\rm overdrive}$   $^{1\!\!/}\,V_{GS}$ –  $V_{th}$   $^{1\!\!/}\,2$  V) as before passivation and comparable on-state DC drain currents.

Figure 4(a) shows the measured output curves for the passivated device by the DC and double pulse (200 ns pulse width) technique using  $V_{GS,q}$  ½ -1.5 V and  $V_{DS,q}$  ½ 0 V. We do not observe any current collapse due to DC-RF dispersion for all pulse widths (not shown here). At 200 ns pulse widths, the drain current is increased by 50% compared to DC at higher drain biases. This demonstrates that Si<sub>3</sub>N<sub>4</sub> passivation can mitigate current collapse in AlGaO/GaO HFETs. Similar result was observed for gate lag measurements too. Even at 200 °C, no current collapse was observed (see the supplementary material). Surprisingly, pulsed measurements show higher currents than DC even at lower drain biases. This is observed for all pulse widths (see the supplementary material). This effect could be due to the effect of traps in the drain access region, which were likely introduced in the Si<sub>3</sub>N<sub>4</sub> deposition process.

Figure 4(b) compares the DC-RF dispersion of the passivated HFET at different quiescent bias conditions as a function of the pulsed width. Current dispersion was compared at V<sub>GS</sub> ¼ 1V and V<sub>DS</sub> ¼ 7V bias points, which has the highest I<sub>D</sub>. Most bias conditions, including the high  $V_{GD}$  pinch off condition ( $V_{GS,q} \frac{1}{4}$  -1V and  $V_{DS,q} \frac{1}{4}$  7 V), I<sub>DPulse</sub> are higher than the DC value, and the reduced pulse width increases the current, indicating effective passivation of the traps in the gate-drain access region that caused current collapse before passivation. The pulsed drain current increases continuously compared to DC at lower pulse widths due to the reduced self-heating effect in addition to the traps that cause current increase seen at lower drain biases. Only when both drain and gate quiescent bias conditions are set to high (V<sub>GS,q</sub> ¼ 1 V and V<sub>DS,q</sub> ¼ 7 V), a small current collapse is seen. This is attributed to the heating effect rather than any trapping effect as the traps are likely filled in the on-state. This is verified by using lower V<sub>DS,q</sub> ¼ 5 V, which resulted in smaller dispersion than  $V_{DS,q}$  ¼ 7 V. Double pulsed  $I_{DS}$ – $V_{GS}$  transfer curves (see the supplementary material) after passivation do not show any change in the threshold voltage ruling out traps under the gate, 14,19,28 although further studies are necessary to completely rule this out.

Temperature dependent RF measurements were carried out on un-passivated and passivated HFETs using an ENA 5071C vector network analyzer (VNA) from 100 MHz to 19 GHz with CPW probes. The VNA was calibrated using an alumina standard substrate at each temperature. An on-wafer open structure was measured at each temperature and used to de-embed the parasitic capacitance from contact pads. Figures 5(a) and 5(b) show  $f_T$  and  $f_{MAX}$  at two different temperatures before passivation. The lower gate length ( $L_G$  160 nm) device has a higher  $f_T$  [Fig. 5(a)], while the longer gate length ( $L_G$  1720 nm) device gave higher  $f_{MAX}$  [Fig. 5(b)] due to lower gate resistance. The pre-passivation RF measurements were limited to  $V_{DS}$  175 V to protect the devices. Figure 5(c) shows the temperature dependent  $f_T$ , and it does not degrade significantly with increasing temperatures. A peak  $f_T$  of 13 GHz is measured at 250 °C. Figure 5(d) shows

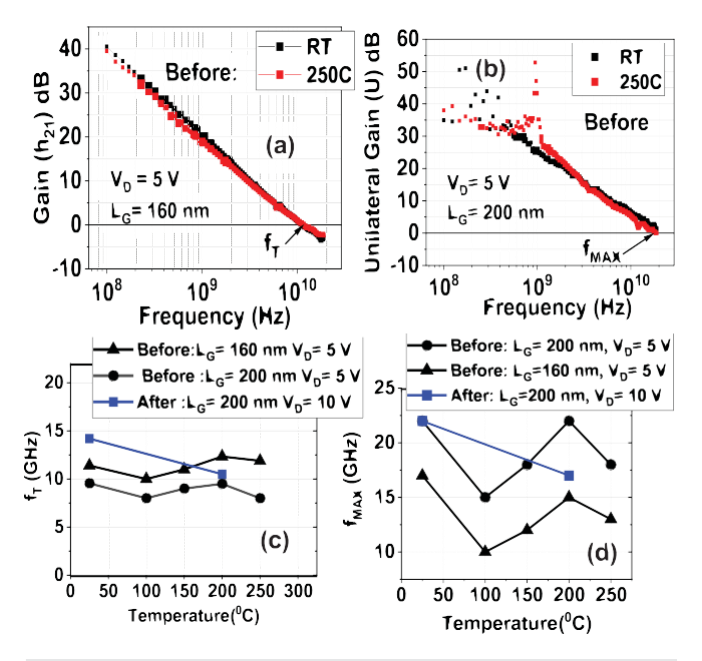


FIG. 5. (a) Measured small signal gain ( $h_{21}$ ) at room temperature and 250 °C before passivation, (b) unilateral gain plot showing  $f_{MAX}$  at two different temperature before passivation, (c) comparison of  $f_T$  before and after passivation for two devices at different bias points, and (d) measured  $f_{MAX}$  for two devices before and after passivation.

the temperature dependent  $f_{MAX}$ , and a peak value of 22 GHz is measured at 200 °C. Figures 5(c) and 5(d) also show the  $f_T$  and  $f_{MAX}$  of a 200 nm gate length device (160 nm  $L_G$  device was destroyed in the passivation and RIE process) after passivation (see the supplementary material for detailed plots), and the values and trend are similar to before passivation, thus showing the suitability of the  $Si_3N_4$  passivation.

In conclusion, a study of the temperature dependent pulsed IV characterization of b-(Al<sub>x</sub>Ga<sub>1-x</sub>)<sub>2</sub>O<sub>3</sub>/Ga<sub>2</sub>O<sub>3</sub> HFETs was carried out. The DC-RF dispersion or current collapse in the gate lag measurements were lower than recessed channel MOSFETs due to the absence of any RIE damage to the channel. A moderate current collapse was observed before passivation. PECVD deposited Si<sub>3</sub>N<sub>4</sub> passivation eliminated current collapse in the AlGaO/GaO HFETs. Pulsed measurements of the passivated devices show a 50% enhancement in the drain current at high drain biases due to reduced self-heating. Dispersion free operation was maintained even at higher temperatures. However, the 350 °C Si<sub>3</sub>N<sub>4</sub> deposition changed the DC characteristics including the threshold voltage on currents and contact linearity. Additionally, different types of traps are introduced, which increase pulsed currents. Further optimization of the Si<sub>3</sub>N<sub>4</sub> deposition process is needed for reliable passivation that does not impact the DC parameters. High frequency characterization up to 250 °C has been demonstrated for b-Ga<sub>2</sub>O<sub>3</sub> HFETs. Negligible degradation of f<sub>T</sub> and f<sub>MAX</sub> at high temperatures is seen for both unpassivated and passivated devices. These results show viability of Ga<sub>2</sub>O<sub>3</sub> devices for high temperature RF applications.

See the supplementary material for details on the  $I_D$ – $V_G$  transfer curve before and after passivation, high temperature pulsed IV and RF

measurement after passivation plots, and peak gm as a function of pulse width analysis.

We acknowledge the support from AFOSR (Air Force Office of Scientific Research) under Award No. FA9550-18-1-0479 (Program Manager: Ali Sayir), from NSF under Award No. ECCS 2019749, from Semiconductor Research Corporation under GRC Task ID 3007.001, and the II-VI Foundation Block Gift Program. This work used the electron beam lithography system acquired through NSF MRI Award No. ECCS 1919798.

#### AUTHOR DECLARATIONS

#### Conflict of Interest

The authors have no conflicts to disclose.

#### DATA AVAILABILITY

The data that support the findings of this study are available from the corresponding author upon reasonable request.

#### REFERENCES

- <sup>1</sup>M. Higashiwaki and G. H. Jessen, "Guest editorial: The dawn of gallium oxide microelectronics," Appl. Phys. Lett. 112,060401 (2018).
- <sup>2</sup>B. Baliga, "Power semiconductor device figure of merit for high-frequency applications," IEEE Electron Device Lett. 10,455-457 (1989).
- <sup>3</sup>K. Zeng, A. Vaidya, and U. Singisetti, "1.85 kV breakdown voltage in lateral field-plated b-Ga<sub>2</sub>O<sub>3</sub>," IEEE Electron Device Lett. 39, 1385-1388
- <sup>4</sup>S. Sharma, K. Zeng, S. Saha, and U. Singisetti, "Field-plated lateral Ga<sub>2</sub>O<sub>3</sub> MOSFETs with polymer passivation and 8.03 kV breakdown voltage," IEEE Electron Device Lett. 41,836-839 (2020).
- <sup>5</sup>A. Bhattacharyya, P. Ranga, S. Roy, C. Peterson, F. Alema, G. Seryogin, A. Osinsky, and S. Krishnamoorthy, "Multi-kV class b-Ga<sub>2</sub>O<sub>3</sub> MESFETs with a lateral figure of merit up to 355 mw/cm<sup>2</sup>," IEEE Electron Device Lett. 42,
- <sup>6</sup>Z. Hu, K. Nomoto, W. Li, N. Tanen, K. Sasaki, A. Kuramata, T. Nakamura,
- D. Jena, and H. G. Xing, "Enhancement-mode Ga<sub>2</sub>O<sub>3</sub> vertical transistors with breakdown voltage >1 kV," IEEE Electron Device Lett. 39, 869-872 (2018).
- X. Huang, F. Liao, L. Li, X. Liang, Q. Liu, C. Zhang, and X. Hu, "3.4 kV breakdown voltage Ga<sub>2</sub>O<sub>3</sub> trench Schottky diode with optimized trench corner radius,"ECS J. Solid State Sci. Technol. 9,045012 (2020).
- <sup>8</sup>K. Ghosh and U. Singisetti, "Ab initio velocity-field curves in monoclinic b-Ga<sub>2</sub>O<sub>3</sub>,"J. Appl. Phys. 122, 035702 (2017).
- <sup>9</sup>Z. Xia, H. Xue, C. Joishi, J. Mcglone, N. K. Kalarickal, S. H. Sohel, M. Brenner, A. Arehart, S. Ringel, S. Lodha, W. Lu, and S. Rajan, "b-Ga<sub>2</sub>O<sub>3</sub> delta-doped field-effect transistors with current gain cutoff frequency of 27 GHz," IEEE Electron Device Lett. 40, 1052–1055 (2019).
- <sup>10</sup>A. J. Green, K. D. Chabak, M. Baldini, N. Moser, R. Gilbert, R. C. Fitch, G. Wagner, Z. Galazka, J. Mccandless, A. Crespo, K. Leedy, and G. H. Jessen, "b-Ga<sub>2</sub>O<sub>3</sub> MOSFETs for radio frequency operation," IEEE Electron Device Lett.
- $\stackrel{11}{\text{A}}\stackrel{38}{\text{C}}\stackrel{790}{\text{C}}\stackrel{793}{\text{C}}\stackrel{(2017)}{\text{S}}$  and U. Singisetti, "Enhancement mode b-(Al $_x$ Gal $_x$ ) O /
- Ga<sub>2</sub>O<sub>3</sub> heterostructure FET (HFET) with high transconductance and cutoff frequency," IEEE Electron Device Lett. 42, 1444–1447 (2021).
- <sup>12</sup>J. Joh, J. A. Del Alamo, and J. Jimenez, "A simple current collapse measurement technique for GaN high-electron mobility transistors," IEEE Electron Device Lett. 29, 665–667 (2008).
- <sup>13</sup>M. Faqir, G. Verzellesi, A. Chini, F. Fantini, F. Danesin, G. Meneghesso, E. Zanoni, and C. Dua, "Mechanisms of RF current collapse in AlGaN-GaN high electron mobility transistors," IEEE Trans. Device Mater. Reliab. 8, 240-247 (2008).

- <sup>14</sup>G. Meneghesso, M. Meneghini, D. Bisi, I. Rossetto, A. Cester, U. K. Mishra, and E. Zanoni, "Trapping phenomena in AlGaN/GaNHEMTs: A study based on pulsed and transient measurements," Semicond. Sci. Technol. 28, 074021
- 15 J. M. Tirado, J. L. Sanchez-Rojas, and J. I. Izpura, "Trapping effects in the transient response of AlGaN/GaN HEMT devices," IEEE Trans. Electron Devices 54,410-417 (2007).
- <sup>16</sup>M. H. Wong, K. Sasaki, A. Kuramata, S. Yamakoshi, and M. Higashiwaki, "Field-plated Ga<sub>2</sub>O<sub>3</sub> MOSFETs with a breakdown voltage of over 750 V," IEEE Electron Device Lett. 37, 212–215 (2016).
- <sup>17</sup>N. A. Moser, J. P. McCandless, A. Crespo, K. D. Leedy, A. J. Green, E. R. Heller, K. D. Chabak, N. Peixoto, and G. H. Jessen, "High pulsed current density b-Ga<sub>2</sub>O<sub>3</sub> MOSFETs verified by an analytical model corrected for interface charge," Appl. Phys. Lett. 110, 143505 (2017).
- <sup>18</sup>N. A. Moser, T. Asel, K. J. Liddy, M. Lindquist, N. C. Miller, S. Mou, A. Neal, D. E. Walker, S. Tetlak, K. D. Leedy et al., "Pulsed power performance of b-Ga<sub>2</sub>O<sub>3</sub> MOSFETs at L-band," IEEE Electron Device Lett. 41, 989-992
- 19 M. Singh, M. A. Casbon, M. J. Uren, J. W. Pomeroy, S. Dalcanale, S. Karboyan, P. J. Tasker, M. H. Wong, K. Sasaki, A. Kuramata, S. Yamakoshi, M. Higashiwaki, and M. Kuball, "Pulsed large signal rf performance of field-plated Ga<sub>2</sub>O<sub>3</sub>MOSFETs," IEEE Electron Device Lett. 39, 1572–1575 (2018).
- <sup>20</sup>J. F. McGlone, Z. Xia, Y. Zhang, C. Joishi, S. Lodha, S. Rajan, S. A. Ringel, and A. R. Arehart, "Trapping effects in Si d-doped b-Ga<sub>2</sub>O<sub>3</sub> MESFETs on an Fe-doped b-Ga<sub>2</sub>O<sub>3</sub> substrate," IEEE Electron Device Lett. 39, 1042-1045
- <sup>21</sup>J. F. McGlone, Z. Xia, C. Joishi, S. Lodha, S. Rajan, S. Ringel, and A. R. Arehart, "Identification of critical buffer traps in Si d-doped b-Ga<sub>2</sub>O<sub>3</sub> MESFETs," Appl. Phys. Lett. 115, 153501 (2019).
- <sup>22</sup>C. Joishi, Z. Xia, J. McGlone, Y. Zhang, A. R. Arehart, S. Ringel, S. Lodha, and S. Rajan, "Effect of buffer iron doping on delta-doped b-Ga<sub>2</sub>O<sub>3</sub> metal semiconductor field effect transistors," Appl. Phys. Lett. 113, 123501 (2018).
- <sup>23</sup>C. Joishi, Z. Xia, J. S. Jamison, S. H. Sohel, R. C. Myers, S. Lodha, and S. Rajan, "Deep-recessed b-Ga<sub>2</sub>O<sub>3</sub> delta-doped field-effect transistors with in situ epitaxial passivation," IEEE Trans. Electron Devices 67,4813-4819 (2020).
- <sup>24</sup>G. Meneghesso, G. Verzellesi, R. Pierobon, F. Rampazzo, A. Chini, U. K. Mishra, C. Canali, and E. Zanoni, "Surface-related drain current dispersion effects in AlGaN-GaN HEMT," IEEE Trans. Electron Devices 51, 1554-1561
- - Trans. Electron Devices 68, 3755–3761 (2021).
- <sup>26</sup>A. Vaidya, J. Sarker, Y. Zhang, L. Lubecki, J. Wallace, J. D. Poplawsky, K. Sasaki, A. Kuramata, A. Goyal, J. A. Gardella, and U. Singisetti, "Structural, band and electrical characterization of b-(Al $_{0.19}$ Ga $_{0.81}$  $_2$ O $_3$  films grown by molecular beam epitaxy on Sn doped b-Ga<sub>2</sub>O<sub>3</sub> substrate," J. Appl. Phys. 126, 095702 (2019).
- <sup>27</sup>S. C. Binari, P. Klein, and T. E. Kazior, "Trapping effects in GaN and SiC microwave FETs,"Proc. IEEE 90, 1048-1058 (2002).
- <sup>28</sup>M. Meneghini, N. Ronchi, A. Stocco, G. Meneghesso, U. K. Mishra, Y. Pei, and E. Zanoni, "Investigation of trapping and hot-electron effects in GaN HEMTs by means of a combined electrooptical method," IEEE Trans. Electron Devices 58,2996-3003 (2011).
- <sup>29</sup>N. A. Blumenschein, N. A. Moser, E. R. Heller, N. C. Miller, A. J. Green, A. Popp, A. Crespo, K. Leedy, M. Lindquist, T. Moule et al., "Self-heating characterization of b-Ga<sub>2</sub>O<sub>3</sub> MOSFETs by pulsed IV and Raman nano-30thermography," IEEE Trans. Electron Devices 67, 204–211 (2019).
- R. Vetury, N. Q. Zhang, S. Keller, and U. K. Mishra, "The impact of surface states on the DC and RF characteristics of AlGaN/GaN HFETs," IEEE Trans. Electron Devices 48, 560-566 (2001).
- <sup>31</sup>A. Vertiatchikh, L. Eastman, W. Schaff, and I. Prunty, "Effect of surface passivation of AlGaN/GaN heterostructure field-effect transistor," Electron. Lett. 38,
- <sup>32</sup>S. C. Binari, K. Ikossi, J. A. Roussos, W. Kruppa, D. Park, H. B. Dietrich, D. D. Koleske, A. E. Wickenden, and R. L. Henry, "Trapping effects and microwave power performance in AlGaN/GaN HEMTs," IEEE Trans. Electron Devices 48, 465-471 (2001).

- <sup>33</sup>H. Kim, R. M. Thompson, V. Tilak, T. R. Prunty, J. R. Shealy, and L. F. Eastman, "Effects of sin passivation and high-electric field on AlGaN-GaN HFET degradation," IEEE Electron Device Lett. 24, 421–423 (2003).
- <sup>34</sup>C. A. Ihalawela, M. Sundararajan, K. W. Cooper, M. E. Kordesch, D. C. Ingram, X.-M. Lin, and G. Chen, "Au and Pt diffusion in electrodeposited amorphous Sb<sub>2</sub>Te<sub>3</sub> thin films," Phys. Status Solidi B 258, 2000428 (2021).
- <sup>35</sup>C. Joishi, Y. Zhang, Z. Xia, W. Sun, A. R. Arehart, S. Ringel, S. Lodha, and S. Rajan, "Breakdown characteristics of b-(Al<sub>0.22</sub>Ga<sub>0.78</sub>)<sub>2</sub>O<sub>3</sub>/Ga<sub>2</sub>O<sub>3</sub> field-plated modulation-doped field-effect transistors," IEEE Electron Device Lett. 40, 1241–1244 (2019).
- <sup>36</sup>M. Koolen, J. Geelen, and M. Versleijen, "An improved de-embedding technique for on-wafer high-frequency characterization," in Proceedings of the 1991 Bipolar Circuits and Technology Meeting, 1991.